Retracing Positions of Terrestrial Laser Scanners to Reinstate Legacy Point Clouds

Felix Eickeler, André Borrmann
Chair of Computational Modelling and Simulation
Technical University of Munich, Germany
felix.eickeler@tum.de

Abstract. Laser scanners provide a mostly geometric representation, but further details can be collected by analysing the recording setup. While the recording configuration is needed in post-processing, it is generally not passed on to the engineers as most scans are created by surveyors and handled by subcontractors. This disconnection between the consumer and the creator can be observed by the fact, that most laser scanned point clouds include intensity information. In day to day use, the intensity information serves as a substitute for colour as it provides contrasts between different objects in the recording. However, from the technical perspective the intensity is the result of the recording device interacting with the surface. This interaction should not be used for automation as different recording setups may result in different interactions and outcomes. Facing this problem, we propose a mechanism to enrich terrestrial laser scans by recreating original scan parameters and further converting the intensity to reflectivity - a sole property of the recorded surface.

1. Introduction

Modern workflows for urban redevelopment, redesign and construction in existing context are based on construction plans and surveys. While surveys do not provide design information or internal specifications, they capture the current state of the area and provide a unified representation. As full geometric models can be abstracted, recent survey techniques promote point clouds instead of control networks as a preferred way for data acquisition. These recordings provide high precision, accuracy and resolution and are a starting point for numerous investigations. Investigations, that can be performed before decisions on new designs need to be finalized. Exploring different variants and clearing issues early, can lead to more efficient building design and better-informed decisions. Ultimately, this results in cost and time savings.

While point clouds can be recorded with different devices, the current gold standard for precise measurements is the terrestrial laser scanner (*TLS*). Mobile laser scanner (*MLS*) have advantages in coverage and recording speed, but the recording complexity is much higher and precise control points are needed. A control network is an additional step with the recording complexity of a full *TLS* scan. With an increasing market for *TLS* surveys, the number of data formats and standards for encoding have prospered, making switches between software and vendors obnoxiously difficult. The interface between different contractors is often the reason for data loss in point clouds. If attributes are not requested and paid by the first contractor, later contractors will receive incomplete point clouds. In many recorded datasets, filters such as voxel grids, have been applied to reduce the load on systems and are steps in the post processing. Nonetheless, automatic remodelling and quality assessment tools might use all information to achieve the best

possible results. Re-engineering of information may be of particular interest for the numerous buildings that were recorded in the past years. These legacy point clouds do not contain needed information as they were neither needed nor requested during the time.

The focus of this research are material properties of the underlying construction. Each material has a distinct reflection signature that can be partially measured by the laser scanner as it is encoded in the intensity (Allmen, 1987). With the correct positioning of the scanner, parts of the material properties can be estimated. However, as the positions of the scanners often are not encoded and lost after merging multiple scans to a single point cloud, the lack of scanning positions needs to be addressed first. Therefore, we will present our approach to recover *TLS* positions and assign all points to their source. In a second step, the reflectivity of the material is calculated. The developed algorithms are benchmarked using datasets consisting of artificial and real-world examples.

2. Related Work

2.1 Terrestrial Laser Scanner

Laser scanners illuminate a target with a concurrent beam and measure the time of flight to deduce the distance. *TLSs* consist of a mirror with two degrees of freedom that redirects the beam (see Figure 1), in different angles. The mirror tilts step by step providing an up-down-shift using primary axis φ and a rotation using the secondary axis θ. The resolution of the scanner relates to the number of positions of the mirror during the recording and can be described by defining the horizontal- and vertical line resolution. The resulting point pattern resembles ripples in water (see Figure 1).

The scanner is controlling the mirror with a fixed angular resolution. As a result, the point density decrease if an object is farther away. Aside from the distance measurement, determined by the speed of light, scanners usually record the signal strength known as intensity. Since *TLSs* record from fixed positions, obstructed elements are not recorded. This behaviour is similar to a point light source. To avoid shadows, multiple aligned scans are combined to a single dataset by using targets that are captured from multiple positions. Merging multiple scans blurs the radial density behaviour. Hot-spots occur close to the scanner pose and objects that are recorded by all scanners are represented with elevated density. New methods propose an adaptive scanning process, to generate a more even distribution based the recording distance (Li et al., 2019).

2.2 Intensity, Reflectivity & Accuracy

Merging multiple scans into a single point cloud has severe consequences for the intensity information. The intensity is mostly affected by the recording distance, the angle of incidence, and the reflectivity of the material. Therefore, intensity information can be considered a property of the recording vector rather than a property of the recorded point. The intensity is usually stored in dimensionless values that depend of the manufacturer of the scanner. Typical values are

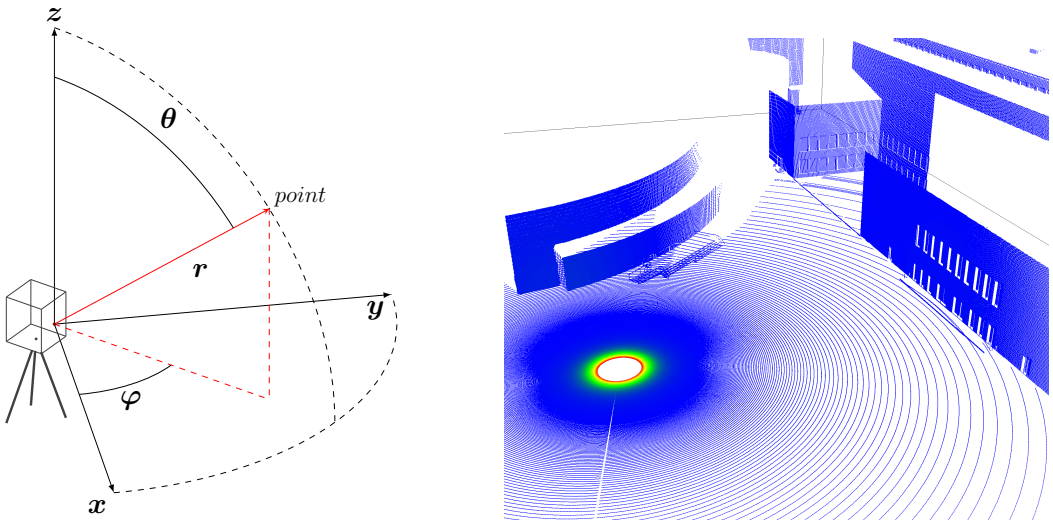

Figure 1: **(a) TLS System.** The scanner records in a spherical coordinate system. In post processing, all points are translated to global space. **(b) Simulation of a Laser Scan.** Colours reflect the density of the scan. With increasing distance, the distance between the horizontal and vertical lines is increasing (Bechtold and B. Höfle, 2016).

$i \in \{[-1;1],\ [0;1],\ [0;1024),\ (-2048;2048)\}$. The propagation of the signal strength can be described by the radar equation (Jelalian, 1992; Kaasalainen et al., 2011):

$$P_r = \underbrace{\frac{P_t D_r^2}{4\beta_t^2}}_{=constant} \frac{\sigma}{\pi r^4} \tag{1}$$

where:

P_t is the transmitted
P_r the received power.
D_r is the aperture of the scanner,
r the distance to the measured point
σ the corss-section backscatter
$|\boldsymbol{p} - \boldsymbol{pos}|$ and β_t the width of the beam.

Under the assumption that the scan parameters were not changed during the scan, we can introduce a constant parameter c_{scan}. Since σ is proportional to the area πr^2 and the incident angle α, the relation can be simplified further:

$$\rho = \frac{r^2\ P_r}{c_{scan}\ cos(\alpha)} \tag{2}$$

The incident angle α can be determined using the surface normal and the recording angle. Based on different surface properties this simple model can be extended to include diffuse and specular reflections (Pfeifer et al., 2007). A benchmark of different reflection models was done by Bolkas (2019) who recommends the Torrance-Sparrow model in combination with the Trowbridge-Reitz distribution (Trowbridge and Reitz, 1975).

If the scanner position is known, such information can be leveraged for multiple applications: (1) Analysis of range precision (Pawłowicz, 2018; Schmitz et al., 2019); (2) Classification of materials(Voegtle, Schwab, and Landes, 2008); (3) Segmentation of point clouds (Bernhard Höfle and Pfeifer, 2007; Levashev, 2019); (4) Filtering & Compression (Eickeler and Borrmann, 2019; Han et al., 2017).

2.3 Edge Detection

Isolating and categorizing points is one of the major tasks in point cloud processing. In images, edges can be detected using the Sobel or Canny edge detection algorithms. For point clouds with a comparable row and column structure (e.g. depth maps), these algorithms have both been successfully implemented (Choi, Trevor, and Christensen, 2013). Known as organized points clouds, these image-like structures resemble the recording of sensors such as RGB-D cameras or single TLS frames.

If point clouds are sparse and randomly ordered, different approaches need to be taken (Hackel, Wegner, and Schindler, 2016; Weber, Hahmann, and Hagen, 2011). One of the main components of many contour detectors is the use of a principle component analysis and the resulting eigenvalues ($\lambda_1, \lambda_2, \lambda_3$).

2.4 Shape Detection in Point Clouds

Another important task is searching and identifying objects. Two general approaches are the Random Sample Consensus (RANSAC) and the Hough Transformation.

RANSAC. The algorithm is based on creating random subsets of points, fitting and testing them against a given model (Lazebnik, 2009; Strutz, 2016). If the deviation, usually root mean squared (RMS) error, is lower than our confidence interval the current set of samples are part of the identified model. Normally the consensus samples are retested and improved iteratively. Because the algorithm is evaluating many different combinations of points, it is known to be a robust and noise resistant method for identifying objects in images and point clouds.

Hough Transform. Another way of fitting a model into a set of samples is the Hough Transformation (*HT*) (Lazebnik, 2009). The underlying data is transformed to a Hough Domain, where each features of the model is parametrized and intersects in a single point. The intersection represents one set of correct parameters. The search space is dependent on the number of free parameters of the model. An example for a *HT* is shown in Figure 2.

For line detection usually the Hesse normal form is used $r = x \cos\theta + y \sin\theta$ and the search parameters is θ (Duda and Hart, 1972). The intersection of all considered points in the $r,\ \theta$-space indicate the parameters of a line. Multiple intersections indicate multiple lines, however the certainty of the line existence decreases as the "intersection to sample ratio" lowers.

During the implementation of the *HT*, the parameter space is discretized. Each sample in the dataset is mapped to the discrete parameter space and added to an accumulator. The accumulator can be thought of as bucket that collects votes on the discretized parameters. For each possible parameter, the model is evaluated and stored in that bucket. After processing all samples, the accumulator will have collected the most certain locations of the model occurring.

Ellipse Hough Transform. The concept of the *HT* can be used to identify circles and ellipses. For circles, the search space consists of 3 dimensions (x, y, r), hence the accumulator is also of 3 dimensions. This makes choosing the appropriate grid size complicated. One approach is separating the accumulator for each search parameter (Yuen, Princen, et al., 1989).

Extending the search to ellipses, the number of dimensions increases to 5 (Hassanein et al., 2015). Different approaches have been made to reduce the size of the accumulator. Yuen, Illingworth, and Kittler (1988) proposed a multi-stage approach, where the centre is identified independently

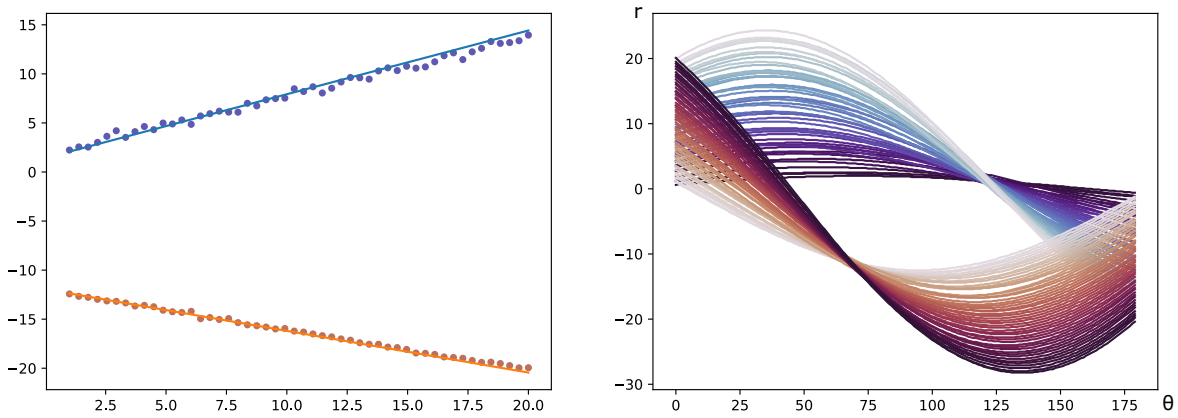

Figure 2: **(a) Line Fitting.** Points Samples of two lines. Both lines are exposed to noise. The drawn lines are the result of the Hough Transformation. (b) **Hough Space.** Each sample point votes on possible angles. The votes gather on two prominent line parameters (intersections).

from the remaining parameters. A more recent approach is the evaluation of point combinations to reduce dimensions. Similar to the RANSAC, the algorithm selects a subset of 3 samples to vote for possible ellipses. The accumulator is left to be purely 1-dimensional (Xie and Ji, 2012).

Hough Transformation in 3D. Some approaches have been made to adapt the *HT* into 3D space. One major concern is the isolation of points of interest. Some *HT* variants for plane and line detection in point clouds exists (Hulik et al., 2014; Khoshelham, 2007; Leeuwen, Coops, and Wulder, 2010; Rabbani and Heuvel, 2005). Generalized 3D curves on surfaces where detected by Torrente, Biasotti, and Falcidieno (2018). Most approaches use projections to handle the increasing complexity of 3D.

3. Methodology

Our approach to increase the value of a legacy laser scans consists of three main steps: (1) Detecting all *TLSs* recording positions; (2) Associate all points to their origin *TLS*; (3) Calculate the reflectivity with a chosen model (see Figure 3).

The only conditions posed upon the input data is that the points of the recordings where not affected by position altering filters (e.g. voxel grid).

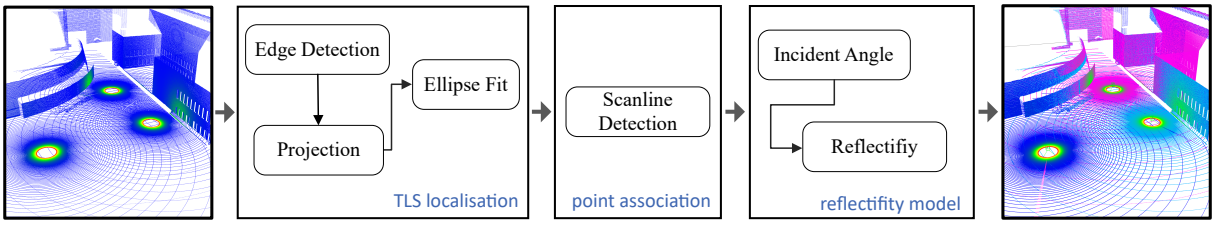

Figure 3: **Process of Enrichment.** The process starts with a non-destructive filtered point cloud. The main process is separated in three parts: analyse, associate, calculate. First, we start the process by identifying contours of interest. We then project the reduced point cloud to the ground and find the centre of recording. In our second step we sort the points based on the recording centres and refine the search. Lastly, we enrich the data by calculating the reflectivity.

3.1 TLS Localisation

The first stage of our analysis is the search for the recording positions. Each scanner has a minimal scanning angle θ_{min} where the tripod is located. In general, surveyors set up the scanner with a spirit level, which results in true horizontal and vertical scan lines. With these two boundary conditions the lowest scan line is typical circular shape on the ground. This circle has a high density due the low distance and is separable from other scan lines. Issues during detection of that circle will occur, if the soil has a gradient or is uneven. The projection of a circle on a sloped ground will form an ellipse. This is also true if the scanner was not set up correctly and the head is tilted.

Edge Detection. Since laser scans are very dense, we need to isolate characteristic shapes in the point cloud before running any parametrization. For effective filtering, a cascade of filters is applied on the second eigenvalue. Based on this eigenvalue evaluations the points with higher λ_2 are culled and outliers are removed based on the mean distance (*SOR*). We then repeat this step until the change of the mean nearest neighbour radius falls under a specific threshold. This approach isolates edges with high densities and strong λ_2 such as the ellipses (see Figure 4).

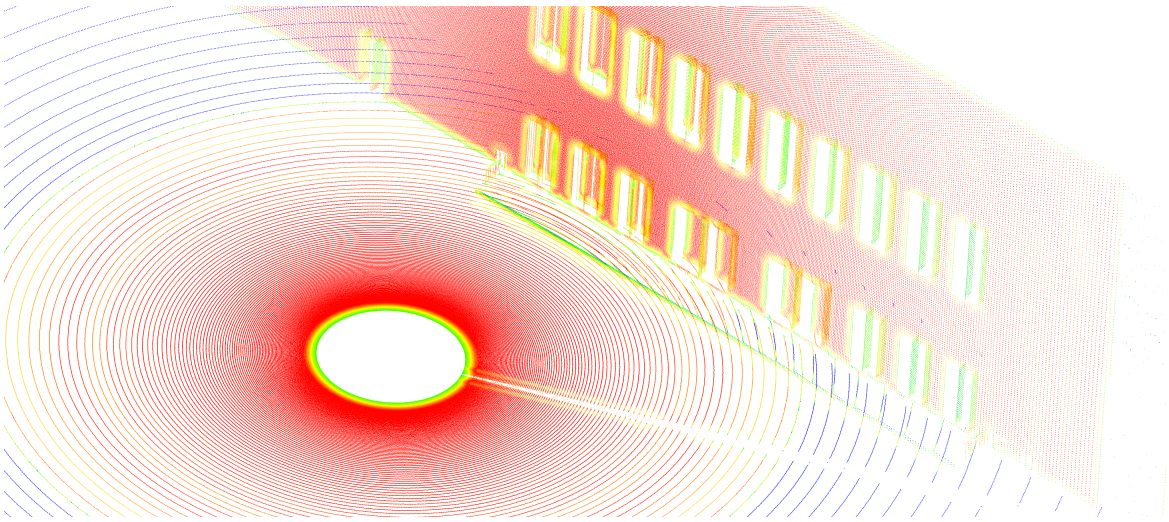

Figure 4: **Edge Detection.** The animation shows the applied cascade of filters; |: λ_2 based filtering; outlier removal :|. The shown example is executed and visualized in CloudCompare (CloudCompare, 2020).

Ellipse Hough Transform. After isolating the edges of possible ellipses, these points are projected to the XY-Plane e.g. the bottom of the bounding box. Following this projection, the 2D space is transferred to the Hough Space by applying an elliptic *HT*. We have chosen the *HT* over any RANSAC implementation as it promises a higher resistance to noise (Jacobs, Weiss, and Dolan, 2013). With multiple scan positions, the ground beneath the tripod is recorded by other scanners and exhibits varying densities.

After testing different approaches for ellipse detection, we decided to use the variant of Xie and Ji (2012) as it performed best in testing and was safe to implement. The chosen algorithm has a worst-case runtime behaviour of $O(n^3)$ and the discretization grid should be rather coarse. If a selected pair reaches the required votes, during calculation, all points belonging to this subset are removed from the global set, reducing the size of calculations for the next ellipse.

After all ellipses are identified, two things are verified: Are the recordings parallel to the XY-Plane and does the assumption hold that the Z-axis is aligned with the gravity vector. If both are correct,

no further corrections are needed. If the XY-Plane is not parallel to the recording plane, the point cloud needs to be projected into the scanner's projected base. This base can be abstracted from the ellipse parameters. In contrast, if all recording planes are parallel to each other but not to the XY-Plane of the scan, we assume to have a non-aligned system. This system can be transformed into a common recording system using any scanners elliptic shape.

Ellipse Refinement. Good performing *TLS* work with trifling angles increments for θ and φ, resulting in small differences between the recorded vertical and horizontal lines. The centre of the ellipse is only as accurate as the discretization of the search space, and cannot be considered accurate enough. Hence refinement is needed. After identifying the *TLS* pose and the ellipse parameters, the original point cloud is transformed into the scanners system (only if needed) and projected to the XY-Plane (2D projection). For each scanner, a grid of $7x7$ is placed around the identified centre (see Figure 5) and lines are identified with a secondary Hough Transform. This times the search is performed with a sufficient big sample size (we used 10 000 points) and has limited search space as the only unknown parameter is the position in the grid. This process of refinement is repeated multiple time with a bisected grid size and increasing minimal distance of the samples. This refinement is repeated until the voting will not determine a clear winner among the grid candidates. The grid cell selected from the previous iteration is considered the most probable TLS location.

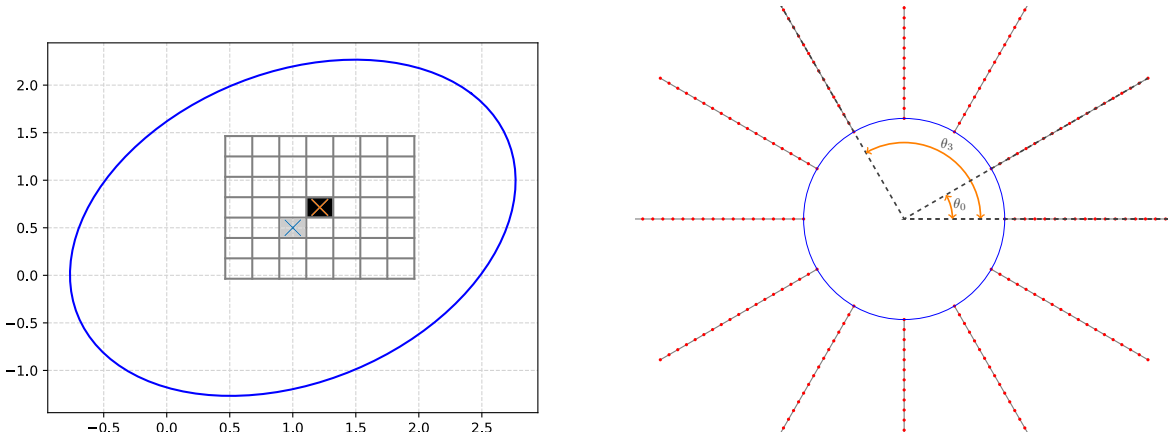

Figure 5: **(a) Refinement.** The initial location is selected based on the elliptic Hough Transform (orange & black). A grid is placed for further refinement. After refinement, the new centre is selected (blue & grey). This process is repeated on finer grid until no grid cell has the majority of votes. **(b) Point Association.** Each point is part of a vertical scan line. All angles are evaluated, and the greatest common divisor is selected.

3.2 Point Assignment

The assignment of points to a scanner is straight forward. The vector of the scan centre to the point is formed and vectors with similar angles φ are detected. If enough points are found, they are assigned to the current scanner. To speed up the process we use a polar grid. After all points have been assigned to a *TLS* position, the θ is used to identify singularities. For each point φ and θ are unique and representative. Furthermore, the greatest common divisor should be the scanners parameter $\Delta\varphi$.

The greatest common divisor is calculated in steps of .05 °. We calculate and collect φ for all points and analyse the separated sets (see Figure 5). Under the assumption that scanners

increment with constant steps size, we check the value with a confidence interval. The line is constructed as:

$$\varphi = \Delta\varphi x - min(\varphi) \tag{3}$$

where x is the array of steps taken.

If points exceed the confidence interval, they are removed from the current scanner. We end up with 3 classes of points: assigned, wrongly assigned, unclassified. Wrongly classified points can be retested to fit into other *TLS* poses. Unclassified points are recording glitches reflecting wrong positions. These points could be reclassified using intensity similarities between their nearest neighbours of different scanners. However, the measurement is not to be trusted.

3.3 Reflectivity Model

As a follow-up to the point assignment, we can calculate the reflectivity. We use the model described in Equation 2. We are creating normals by evaluating patches formed by the nearest neighbours. If the scanners use negative intensity values, the range is shifted to the positive range. Since we cannot estimate Pr from the point cloud data alone, we are left with two possible options: (1) Use the intensity values which will result in a corrected but non-normalized scan; (2) Use surface with known reflectivity values such as targets to calibrate.

4. Results

For verification we use artificial and real-world data: (1) The artificial data was created with Helios applied on an inner city 3D model (Bechtold and B. Höfle, 2016). The simulation resulted in two sets, featuring a one and a three *TLS* position survey. The materials were not defined, resulting in no useful intensity information. The resulting circles of the scanners were close to 5 m in diameter. (2) The real-world test data is snipped of an ongoing construction site which was recorded with a Leica HDS6100 in 2018. The construction site featured overall 8 positions where 3 are in possible range of the selected area. The dataset consists of the properties x, y, z, i and was exported from Leica's Cyclone. During the recording, some equipment was moved and was only recorded by a single scan pose. The measured major axis was 1.3 m.

4.1 TLS Detection

To benchmark our *TLS* detection, we measured the performance of each step individually. We were able to isolate the scanner ellipses in all data sets. For the artificial set, the contour search is visualized in the animation Figure 4). The filtering was concluded after 10 iterations for the single scanner, 12 for the three scanner and only 7 for the real dataset. However, the number of points was reduced to 2.5 % for the artificial data and <1% for the real-world data (see Figure 6. The difference is due the different density settings of the scanner, and the fixed number of nearest neighbours considered by the outlier filter.

Despite our effective isolation of the edge detection, the calculation is intensive. Both of our test datasets provide close to perfect circular shapes, which simplified the process as there was no need for further transformations. The results of the ellipse fit can be seen in Table 1. The centre

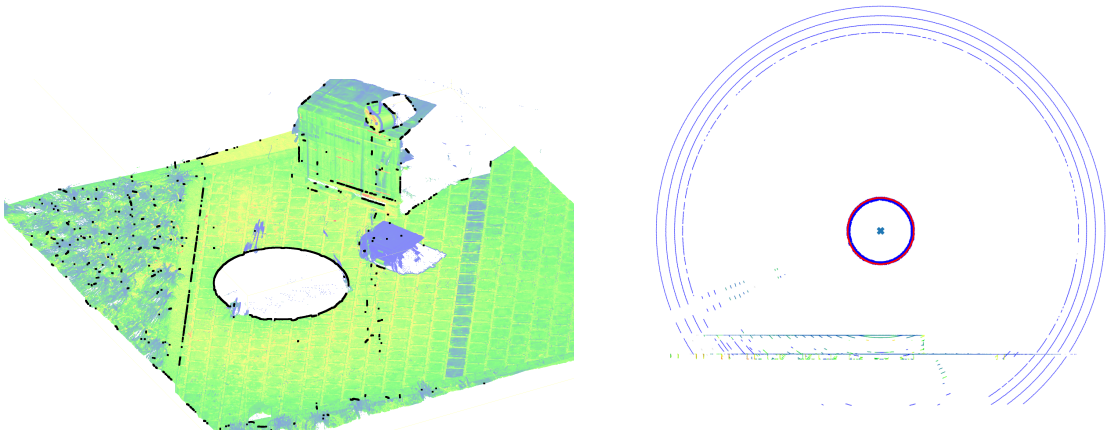

Figure 6: **(a) Contour Isolation.** The contours are overlaid (black) to the original real-world point cloud. Aside from the ellipse, only the edge to the cobbles is remaining. **(b) TLS Ellipse Fit.** The image shows the birds-eye view on the reduced point cloud in Figure 4. The ellipse was fitted, and the scanner position determined (green). The ellipse formed a perfect circle (red).

Table 1: **Initial Ellipse Fit.** For the real-world data, the points are measured with manual accuracy.

Scanner	original [m]		detected [m]		$\Delta x[mm]$	$\Delta y[mm]$	$\Delta rms[mm]$
1	14.17	-9.57	14.14	-9.57	26	4	26.3
2	8.95	23.14	8.93	23.12	20	16	25.6
3	42.22	-6.92	42.21	-6.93	6	5	7.8
real	51.09	48.06	50.11	48.08	23	19	29.8

of the scanner could be determined with very good accuracy for our artificial dataset as the initial ellipse fit provided an accuracy <27 mm.

4.2 Point Assignment & Reflectivity model

As the noise levels in the artificial dataset are low compared to the real-world example, we were able to assign all points with high confidence. Due the order or processing and the real-world thresholds, few point were assigned to the wrong scanner. The reflectivity was calculated and within expected margins of the standard material. However, it showed outliers at the edges of the dataset. We assume this is due to the low-density settings of the dataset, introducing artefacts in the surface normals. For the real-world dataset, the calculations are still ongoing and will be presented at the conference.

5. Conclusion & Outlook

This paper combined specific Edge Filtering, Hough Transforms, Refinement Search and statistical methods to iteratively retrace the original recording positions. The *TLS* postilions were localized with good accuracy and further scan parameters, such as the line resolution and the recording angles, could be derived. With the reacquired meta-information, we assigned each point to

the origin, which enabled further processing on secondary properties. As a showcase, we implemented a simple reflectivity model and were able to re-evaluate the intensity and resolve the dependency between the recording setup and the point cloud: The scan intensities were renormalized and transformed to position independent values. We further showed, that the given approach is suited for the revaluation of legacy laser scans. The newly obtained information can be used to improve filtering, segmentation, and general point cloud processing.

Additionally to our findings, the concept should be extended with an advanced reflectivity model and a smart classification scheme for materials and surfaces. Material estimations are desired to improve Scan2Bim applications, and filtering. Extending this topic further, the inclusion of colour into the material classifiers will merge another layer of information.

Considering the presented approach, we want to mention that further datasets should be evaluated and benchmarked. Additionally, the evaluation of shading angles and a stochastic surface segmentation model should be implemented. This model may be used to identify fine grained contours and could also be used to re-evaluate outliers. This would create a closed loop system for analysis and increase the robustness compared to the current isolated approach.

References

Allmen, Martin von (1987). *Laser-Beam Interactions with Materials*. Springer Berlin Heidelberg. DOI: 10.1007/978-3-642-97007-8. URL: https://doi.org/10.1007%2F978-3-642-97007-8.

Bechtold, S. and B. Höfle (2016). "HELIOS: A Multi-Purpose LiDAR Simulation Framework for Research, Planning and Training of Laser Scanning Operations with Airborne, Ground-Based Mobile and Stationary Platforms". In: *ISPRS Annals of Photogrammetry, Remote Sensing and Spatial Information Sciences* III-3, pp. 161–168. DOI: 10.5194/isprs-annals-III-3-161-2016.

Bolkas, D. (2019). "Terrestrial laser scanner intensity correction for the incidence angle effect on surfaces with different colours and sheens". In: *International Journal of Remote Sensing* 40.18, pp. 7169–7189. DOI: 10.1080/01431161.2019.1601283.

Choi, Changhyun, Alexander J. B. Trevor, and Henrik I. Christensen (Nov. 2013). "RGB-D edge detection and edge-based registration". In: *2013 IEEE/RSJ International Conference on Intelligent Robots and Systems*. IEEE. DOI: 10.1109/iros.2013.6696558.

CloudCompare (2020). *GPL software*. Version 2.11 alpha. URL: https://www.cloudcompare.org.

Duda, Richard O. and Peter E. Hart (Jan. 1972). "Use of the Hough transformation to detect lines and curves in pictures". In: *Communications of the ACM* 15.1, pp. 11–15. DOI: 10.1145/361237.361242.

Eickeler, Felix and André Borrmann (2019). "Adaptive feature-conserving compression for large scale point clouds". In: *Proc. of the 26th EG-ICE Workshop on Intelligent Computing in Engineering*. Leuven, Belgium.

Hackel, Timo, Jan D. Wegner, and Konrad Schindler (June 2016). "Contour Detection in Unstructured 3D Point Clouds". In: *2016 IEEE Conference on Computer Vision and Pattern Recognition (CVPR)*. IEEE. DOI: 10.1109/cvpr.2016.178.

Han, Xian-Feng et al. (Sept. 2017). "A review of algorithms for filtering the 3D point cloud". In: *Signal Processing: Image Communication* 57, pp. 103–112. DOI: 10.1016/j.image.2017.05.009.

Hassanein, Allam Shehata et al. (2015). "A survey on Hough transform, theory, techniques and applications". In: *arXiv preprint arXiv:1502.02160*.

Höfle, Bernhard and Norbert Pfeifer (2007). "Correction of laser scanning intensity data: Data and model-driven approaches". In: *ISPRS Journal of Photogrammetry and Remote Sensing* 62.6, pp. 415–433. DOI: 10.1016/j.isprsjprs.2007.05.008.

Hulik, Rostislav et al. (Jan. 2014). "Continuous plane detection in point-cloud data based on 3D Hough Transform". In: *Journal of Visual Communication and Image Representation* 25.1. DOI: 10.1016/j.jvcir.2013.04.001.

Jacobs, Lucas, John Weiss, and Dan Dolan (May 2013). "Object tracking in noisy radar data: Comparison of Hough transform and RANSAC". In: *IEEE International Conference on Electro-Information Technology , EIT 2013*. IEEE. DOI: 10.1109/eit.2013.6632715.

Jelalian, A.V. (1992). *Laser Radar Systems*. Artech House radar library. Artech House. ISBN: 9780890065549.

Kaasalainen, Sanna et al. (2011). "Analysis of Incidence Angle and Distance Effects on Terrestrial Laser Scanner Intensity: Search for Correction Methods". In: *Remote Sensing* 3.10, pp. 2207–2221. DOI: 10.3390/rs3102207.

Khoshelham, K. (2007). "Extending generalized hough transform to detect 3D objects in laser range data". In: *Proceedings of the ISPRS workshop Laser Scanning 2007 and SilviLasser 2007, Espoo, Finland, 12-14 September 2007*. International Society for Photogrammetry and Remote Sensing (ISPRS), pp. 206–210.

Lazebnik, Svetlana (2009). *Lecture notes in Computer Vision (COMP 776)*.

Leeuwen, Martin Van, Nicholas C. Coops, and Michael A. Wulder (2010). "Canopy surface reconstruction from a LiDAR point cloud using Hough transform". In: *Remote Sensing Letters* 1.3, pp. 125–132. DOI: 10.1080/01431161003649339.

Levashev, S. P. (2019). "Segmentation of a Point Cloud by Data on Laser Scanning Intensities". In: *Pattern Recognition and Image Analysis* 29.1, pp. 144–155. DOI: 10.1134/s1054661819010152.

Li, Qinghua et al. (2019). "Towards Uniform Point Density: Evaluation of an Adaptive Terrestrial Laser Scanner". In: *Remote Sensing* 11.7, p. 880. DOI: 10.3390/rs11070880.

Pawłowicz, Joanna A. (2018). "Impact of physical properties of different materials on the quality of data obtained by means of 3d laser scanning". In: *Materials Today: Proceedings* 5.1, p. 1997. DOI: 10.1016/j.matpr.2017.11.304.

Pfeifer, Norbert et al. (Jan. 2007). "Investigating terrestrial laser scanning intensity data: quality and functional relations". In: *8th Conference on Optical 3-D Measurement Techniques*.

Rabbani, Tahir and Frank Heuvel (Jan. 2005). "Efficient Hough transform for automatic detection of cylinders in point clouds". In: *Proceedings of the ISPRS workshop Laser Scanning 2005*. Vol. 36. International Society for Photogrammetry and Remote Sensing (ISPRS).

Schmitz, Berit et al. (2019). "How to Efficiently Determine the Range Precision of 3D Terrestrial Laser Scanners". In: *Sensors* 19.6, p. 1466. DOI: 10.3390/s19061466.

Strutz, Tilo (2016). *Data Fitting and Uncertainty*. Springer Fachmedien Wiesbaden. DOI: 10.1007/978-3-658-11456.

Torrente, Maria-Laura, Silvia Biasotti, and Bianca Falcidieno (Jan. 2018). "Recognition of feature curves on 3D shapes using an algebraic approach to Hough transforms". In: *Pattern Recognition* 73, pp. 111–130. DOI: 10.1016/j.patcog.2017.08.008.

Trowbridge, T. S. and K. P. Reitz (May 1975). "Average irregularity representation of a rough surface for ray reflection". In: *Journal of the Optical Society of America* 65.5, p. 531. DOI: 10.1364/josa.65.000531.

Voegtle, T, I Schwab, and T Landes (2008). "Influences of different materials on the measurements of a terrestrial laser scanner (TLS)". In: 37, pp. 1061–1066.

Weber, Christopher, Stefanie Hahmann, and Hans Hagen (2011). "Methods for feature detection in point clouds". In: *Visualization of Large and Unstructured Data Sets-Applications in Geospatial Planning, Modeling and Engineering (IRTG 1131 Workshop)*. Schloss Dagstuhl-Leibniz-Zentrum fuer Informatik.

Xie, Yonghong and Qiang Ji (2012). "A new efficient ellipse detection method". In: *Object recognition supported by user interaction for service robots*. IEEE Comput. Soc. DOI: 10.1109/icpr.2002.1048464.

Yuen, H. K., J. Illingworth, and J. Kittler (1988). "Ellipse Detection using the Hough Transform". In: *Procedings of the Alvey Vision Conference 1988*. Alvey Vision Club. DOI: 10.5244/c.2.41.

Yuen, H. K., J. Princen, et al. (1989). "A Comparative Study of Hough Transform Methods for Circle Finding". In: *Procedings of the Alvey Vision Conference 1989*. Alvey Vision Club. DOI: 10.5244/c.3.29.